Computational and Theoretical Chemistry 1004 (2013) 69–75

Contents lists available at SciVerse ScienceDirect

Computational and Theoretical Chemistry

journal homepage: www.elsevier.com/locate/comptc

Computational study of the intramolecular proton transfer reactions of dipicolinic acid (pyridine-2,6-dicarboxylic acid) and its dimers

Seyed Hasan Kazemi *, Hossein Eshtiagh-Hosseini, Masoud Mirzaei

Department of Chemistry, Ferdowsi University of Mashhad, Mashhad 917751436, Iran

ARTICLE INFO

Article history:
Received 21 June 2012
Received in revised form 19 October 2012
Accepted 31 October 2012
Available online 10 November 2012

Keywords:
Intramolecular proton transfer (IPT)
Electrostatic potential (ESP)
Dipicolinic acid (DPA)
Hydrogen bonding
Zwitterion
Dimer

ABSTRACT

The intramolecular proton transfer (IPT) reaction and dimerization processes of dipicolinic acid (DPA) have been investigated using density functional theory (DFT) at the B3LYP/6-31G++(d) basis set level. The influence of the solvent on the zwitterion -to- neutral transition of DPA was examined using the continuum model (CPCM) with different dielectric constants (ε = 4.9, $CHCl_3$; ε = 7.42, THF; ε = 32.63, CH_3OH; ε = 78.39, H_2O). The intramolecular proton transfer reaction occurs more readily in the gas phase than solution. Results also show that the stability of DPA dimers in the gas phase is directly affected by the hydrogen bond angle and electrostatic potential (ESP) value in the dimer structure.

1. Introduction

Since intramolecular proton transfer (IPT) is one of the most important reactions in many chemical and biological processes, numerous experimental and theoretical studies have been carried out to increase knowledge of the mechanisms of IPT [1–14].

Dipicolinic acid (DPA, pyridine-2,6-dicarboxylic acid, $C_5H_3N(COOH)_2$) was first identified in 1936 as a viscous matter in Natto, a Japanese food made with steamed soybeans and fermented with Bacillus Natto [15]. It was not until 1953 that DPA was first recognized to be a by-product of bacterial spore germination [16,17]. Since then, DPA has been investigated as a potential indicator of bacterial spore formation and germination using a wide range of detection techniques [18–20]. It can protect bacterial spores because of its strong ability to absorb UV light, hence up to 50% of the solids excreted by spores are compounds of DPA. It is well-known to be a molecule with high chelation. Experiments performed on wet paste and dry crystal forms of DPA and CaDPA have shown interesting effects on their fluorescence intensities [21]. Other experimental and theoretical investigations of DPA and its derivatives have been relatively sparse [22–30]. The X-ray structure of DPA shows that the molecules are arranged as one-dimensional supramolecular structure and stabilized in the solid state through a strong symmetric double hydrogen bond [31–33].

The recent study by Massaro and Blaisten-Barojas reports that DPA has six predicted neutral isomers in the gas phase. N (see Fig. 1) is the global minimum structure taking into account that its total electronic energy plus the zero point energy is the lowest of the six predicted structures [34]. Another structure which can exhibit N is the zwitterionic form (Z), in which the nitrogen atom and one of COOH groups become NH^+ and COO^-, respectively [35]. The zwitterionic forms of DPA may be conveniently studied in solution with the suitable pH value [36] and in the presence of an appropriate amine [37–48] or their self-assembled systems [49–61]. Therefore, DPA is a good model compound for *intra*- and *inter*molecular proton transfer studies. The carboxyl protons are involved in the *intra*- and *inter*-molecular hydrogen bonds (the pyridine's nitrogen atom and the carboxyl's oxygen lone pairs can be hydrogen bond acceptors). In this paper, we report the investigation of the IPT reaction between the N and Z structures (see Fig. 1) of DPA. In order to follow the atoms of DPA, they have been numbered in a consistent scheme. By following the Isin's method [6] in this work, we carried out calculations using Becke's Three Parameter Hybrid Functional together with the correlation functional of Lee, Yang, and Parr (B3LYP) methods [62,63] for DPA in the gas phase, chloroform, THF, methanol and water in order to evaluate the effect of the solvent on IPT. Also, computations on DPA dimers with two different structures were performed in the gas phase at the B3LYP/6-31G(d) level. Based on a search of the literature, this is the first computational study of the IPT reaction between two structures of DPA and the hydrogen bonding between their dimers. Therefore, we hope that our study provides an ppenhanced interpretation of DPA as well as its derivatives.

* Corresponding author. Tel.: +98 511 8797022; fax: +98 511 8795457.
E-mail address: kazemi-r@um.ac.ir (S.H. Kazemi).

2210-271X/$ - see front matter © 2012 Elsevier B.V. All rights reserved.
http://dx.doi.org/10.1016/j.comptc.2012.10.024

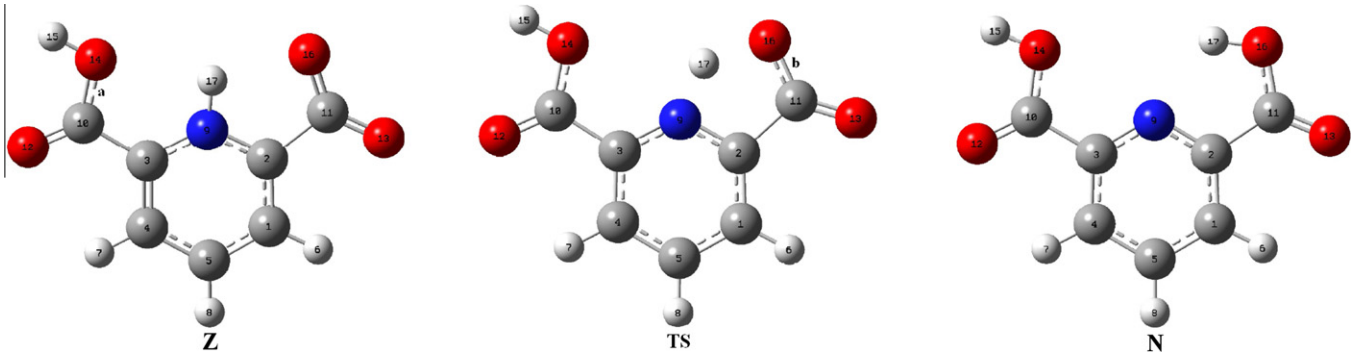

Fig. 1. Optimized molecular structures of N, Z and the transition state (TS). Carbon atoms are colored in gray, oxygen atoms in red, nitrogen atoms in blue, and hydrogen atoms in white. (a) The $C_{10}O_{14}$ bonds are single, in the gas phase (in all forms). (b) The $C_{11}O_{16}$ bond is double, in the gas phase(in TS form).

2. Computational details

The stationary structures (N and Z) in the IPT reaction of DPA and (NN and ZZ) in the dimerization of DPA were optimized using density functional theory (DFT) at the most popular B3LYP method [62,64] and a double-ζ basis set with an extra d polarization function and diffuse functions on all atoms (6-31G++(d)). The vibrational frequencies were obtained at the same level to characterize the local minimum and the transition states (corresponding to a single negative eigenvalue of the Hessian). The non-specific solvent effects of the solvent medium were studied by means of the conductor-polarizable continuum model (CPCM) [65]. The CPCM has been used for energy calculations with a different dielectric constants ($\varepsilon = 4.9$, $CHCl_3$; $\varepsilon = 7.42$, THF; $\varepsilon = 32.63$, CH_3OH; $\varepsilon = 78.39$, H_2O) in the IPT reactions of DPA. The basis set superposition error (BSSE) associated with the hydrogen bond energy in the dimerization of DPA was computed via the counterpoise method using the individual bases as fragments [66]. Also the molecular electrostatic potential (ESP) were calculated for DPA dimers. All the calculations were performed with the Gaussian 09 W package [67].

3. Results and discussion

The B3LYP/6-31G++(d) optimized geometries for N, Z and TS (the transition state) are shown in Fig. 1, and selected structural parameters are listed in Table 1.

The IPT reaction Z → TS → N was considered. The transfer of a hydrogen atom from the N_9 to the O_{16} atom is accompanied by a rearrangement of the six-membered ring, and substantial changes are observed in the carbon—oxygen, nitrogen—hydrogen and oxygen—hydrogen bonds. The distance between H_{17} and O_{16} decreases upon the IPT. The N_9—H_{17} and O_{16}—H_{17} distances for TS are 1.170 Å and 1.438 Å in the gas phase. Compared to initial content of those, it can be concluded that the N_9—H_{17} bond is broken and an O_{16}—H_{17} bond is formed during the IPT process in DPA. During proton transfer Z → TS → N, the C_2—C_{11} and C_{11}—O_{13} distances decrease, the C_3—C_4 and C_{11}—O_{16} distances increase, the C_1—H_6, C_4—H_7, C_5—H_8 and O_{14}—H_{15} distances remain unchanged, the C_1—C_2 distance first decreases and then increases in all phases. The $C_{10}O_{14}$ distance and the $C_2N_9H_{17}$ angle decrease on Z → N transfer, while the angles $C_1C_2N_9$, $C_3C_{10}O_{14}$ and $C_2C_{11}O_{13}$ increase. The angles $C_4C_3N_9$, $C_4C_3C_{10}$, $C_2N_9C_3$, $O_{12}C_{10}O_{14}$, $O_{13}C_{11}O_{16}$ and

Table 1
Selected bond lengths, bond and dihedral angles derived from B3LYP/6-31G++(d) geometric optimization of DPA in the gas and solution phases.

Parameters [a]	Gas phase			Chloroform (ε = 4.9)			THF (ε = 7.42)			Methanol (ε = 32.63)			Water (ε = 78.39)		
	N	TS	Z	N	TS	Z	N	TS	Z	N	TS	Z	N	TS	Z
Distance															
C_1C_2	1.399	1.392	1.398	1.398	1.390	1.395	1.398	1.389	1.394	1.398	1.389	1.394	1.398	1.389	1.394
C_3C_4	1.400	1.393	1.386	1.400	1.395	1.386	1.400	1.395	1.386	1.401	1.396	1.386	1.401	1.396	1.386
C_2C_{11}	1.512	1.552	1.562	1.507	1.536	1.547	1.507	1.535	1.546	1.506	1.533	1.543	1.506	1.533	1.543
$C_{10}O_{14}$	1.347	1.345	1.347	1.343	1.341	1.342	1.343	1.341	1.341	1.342	1.340	1.340	1.342	1.340	1.340
$C_{11}O_{16}$	1.342	1.283	1.256	1.341	1.294	1.258	1.341	1.295	1.258	1.341	1.296	1.258	1.341	1.297	1.258
N_9H_{17}	2.023	1.170	1.043	2.011	1.225	1.031	2.008	1.231	1.030	2.005	1.240	1.029	2.005	1.242	1.028
$O_{16}H_{17}$	0.984	1.438	1.940	0.985	1.341	2.072	0.986	1.331	2.087	0.986	1.319	2.107	0.986	1.316	2.110
$C_{11}O_{13}$	1.211	1.227	1.238	1.215	1.229	1.246	1.216	1.230	1.248	1.216	1.230	1.249	1.217	1.230	1.249
Bond angle															
$N_9C_2C_{11}$	115.69	108.00	113.12	115.19	107.44	114.50	115.12	107.38	114.64	115.03	107.32	114.83	115.01	107.32	114.86
$C_2C_{11}O_{16}$	114.16	108.27	111.01	114.37	108.51	112.96	114.39	108.56	113.20	114.41	108.62	113.54	114.42	108.63	113.60
$O_{13}C_{11}O_{16}$	122.97	132.72	134.58	122.04	129.88	131.66	121.94	129.58	131.29	121.78	129.14	130.78	121.76	129.07	130.68
$C_{10}O_{14}H_{15}$	106.78	108.10	108.69	107.69	108.65	109.50	107.79	108.70	109.59	107.93	108.78	109.71	107.95	108.79	109.74
$C_1C_2N_9$	123.39	120.83	118.76	123.52	121.59	118.61	123.53	121.65	118.60	123.55	121.76	118.59	123.56	121.78	118.59
$C_4C_3N_9$	122.65	119.09	118.69	122.58	119.37	118.84	122.57	119.39	118.88	122.56	119.43	118.91	122.55	119.44	118.92
$C_4C_3C_{10}$	118.72	121.14	121.75	118.95	121.56	122.12	118.98	121.28	122.14	119.03	121.30	122.18	119.04	121.31	122.19
$C_2N_9C_3$	118.35	122.99	124.33	118.28	122.30	124.24	118.27	122.25	124.22	118.26	122.15	124.18	118.26	122.13	124.18
$C_3C_{10}O_{14}$	113.40	112.09	111.56	113.44	112.29	111.56	113.44	112.31	111.53	113.44	112.33	111.52	113.44	112.34	111.52
$O_{12}C_{10}O_{14}$	123.32	124.64	124.94	123.39	124.66	125.31	123.40	124.65	125.38	123.41	124.64	125.44	123.41	124.64	125.45
$C_2C_{11}O_{13}$	122.86	119.01	114.41	123.58	121.61	115.38	123.67	121.86	115.50	123.80	122.24	115.68	123.82	122.30	115.71
$C_2N_9H_{17}$	–	98.37	110.12	–	96.27	113.19	–	96.07	113.51	–	95.80	113.95	–	95.76	114.02

[a] Distances in Å; angles in degrees. For numbering of atoms, see Fig. 1.

$C_{10}O_{14}H_{15}$ decrease, while the angles $N_9C_2C_{11}$ and $C_2C_{11}O_{16}$ first decrease and then increase on Z → TS → N transfer in all phases. The C_2—N_9, C_3—N_9, C_1—C_5, C_4—C_5, C_3—C_{10} and C_{10}—O_{12} distances are fixed, in all non-gas phases.

The total electronic energies of the DPA are given in Table 2. Let's see how the calculated transformation energy for DPA changes. The transformation energy, as shown in Fig. 2, was calculated as the total electronic energies differences between the transition states (TSs) and the initial forms (Z). The relative transformation energies of the TS with respect to Z were calculated to be 2.10, 6.60, 7.25, 8.22 and 8.40 kcal/mol in the gas phase, chloroform, THF, methanol, and water, respectively. The barrier height decreases on going from the water to the gas phase. The total electronic energies differences between the two forms (N and Z) were calculated to be −17.14, −7.50, −6.28, −4.54 and −4.23 kcal/mol in the gas phase, chloroform, THF, methanol, and water, respectively, i.e. N is more stable than Z in the gas phase and solution.

As a result, the IPT reaction between structures Z and N occurs very easily in the gas phase than in solution. Similar two coupled barrier heights were observed for all of the solutions. However, we can conclude that the stronger the dipole moment of the solvent, the higher the barrier to the IPT process.

From the viewpoint of valence theory, the interaction between the lone pair of the acceptor O atom and N—H σ^* orbitals is mainly responsible for the proton transfer. Therefore, the N—H···O angle and the O···H distance (in the Z form) may play important roles in the proton transfer reactions. In most cases, hydrogen bonds with linear N—H···O structures and short hydrogen bond distances are considered to be strong. In Z, the N_9—H_{17}···O_{16} angles are 113.24°, 108.83°, 108.37°, 107.75° and 107.64° in the gas phase, in chloroform, in THF, in methanol, and in water, respectively. Additionally, the N_9—H_{17}···O_{16} hydrogen bond distances of Z form are 1.940 Å, 2.072 Å, 2.087 Å, 2.107 Å and 2.110 Å in the gas phase, chloroform, THF, methanol, and water, respectively. The existence of a strong N_9—H_{17}···O_{16} hydrogen bond in Z shows that the barrier to the IPT may have is low in the gas phase. Another reason for this result is that the distance of N_9 from H_{17} in the TS structure is shortest in the gas phase.

Let's now examine the calculated relative Gibbs free energies (ΔG) and activation Gibbs free energy barriers ($\Delta G^{\#}$) for the IPT reaction of DPA in the gas phase and in solutions. As seen in Table 3, the ΔG for the IPT reaction of DPA is lowest in the gas phase. The $\Delta G^{\#}$ height increases on going from the gas phase to the water. As a result, according to ΔG and $\Delta G^{\#}$, this reaction is thermodynamically and kinetically much favor in the gas phase than in solution. When we look at the calculated ΔE_s and ΔG_s values in Table 4, we see that Z is the more stable of these forms, presumably due to solvent effects. In addition, solvent effects mean that the TS structure in solution is more stable than in the gas phase. Consequently, the energy barrier to IPT reaction increases in solution.

The structural parameters of the dimer structures (NN and ZZ) calculated at the B3LYP/6-31G(d) level are shown in Fig. 3. The optimized geometrical parameters indicate that the two forms (N and Z) are fully planar, in agreement with experimental values. The planarity of these structures is attributed to the strong *intra*- and *inter*-molecular hydrogen bonding and the structure of the DPA ring [33,34,36,61]. Two N molecules bind through two

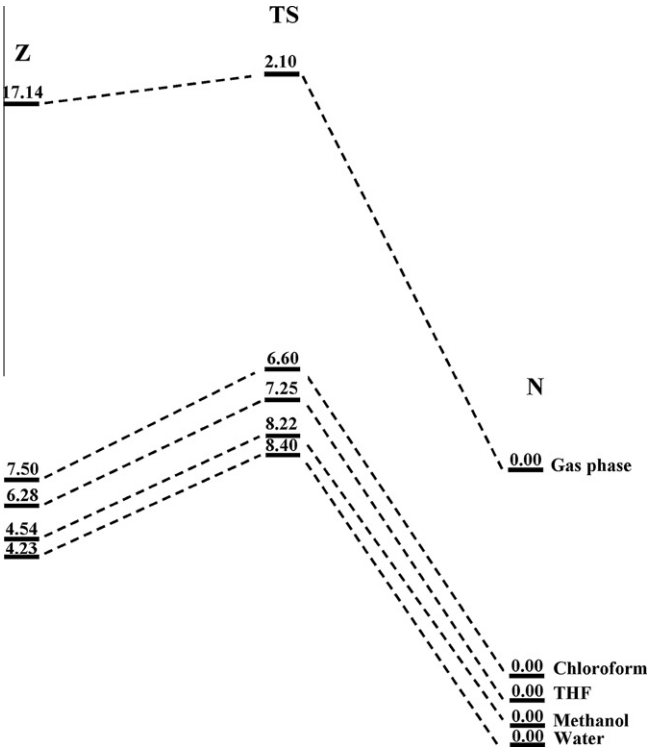

Fig. 2. Energy diagram of the proton transfer process in various solvents (via CPCM) and gas phase.

Table 3
Calculated Gibbs free energies and activation Gibbs free energy barriers (in kcal/mol) for the IPT reaction of DPA.

	ΔG	$\Delta G^{\#}$
Gas phase	−16.54	0.26
Chloroform	−7.54	4.22
THF	−6.37	4.84
Methanol	−4.70	5.75
Water	−4.40	5.92

*inter*molecular hydrogen bonds (O—H···O) joining the COOH groups in the NN structure and similarly in the ZZ structure. These two hydrogen bonds in the dimer structures are equivalent to each other (see Fig. 3). Comparing the monomer and dimer structures in the gas phase, it has been noted that the intermolecular hydrogen bonds affect the molecular structure of the monomer. As seen in Fig. 3, the bond angles and lengths of the hydrogen donor (O—H) and hydrogen acceptor (C=O) groups of the NN and ZZ structures differ from those of their monomers. For example; the $C_3O_{14}H_{15}$ and $O_{12}C_3O_{14}$ angles are increased by 3.81° and 1.45° in NN, respectively. The same angles are increased by 2.94° and 1.02° in ZZ, respectively. Another important point is the changes in the C_3O_{14}, C_3O_{12}, C_3C_{10} and $O_{14}H_{15}$ bond lengths on going from the monomers to the dimeric structures. The results obtained for the gas phase show that the C_3O_{12} and $O_{14}H_{15}$ bond lengths are

Table 2
Total electronic energies (*E*, in hartrees) of the DPA forms in the gas phase and solution at 298.150 K and 1.00000 Atm.

DPA form	$E_{\text{Gas phase}}$	$E_{\text{Chloroform}}$	E_{THF}	E_{Methanol}	E_{Water}
N	−625.45676978	−625.46950255	−625.47092975	−625.47290328	−625.47325028
TS	−625.42610484	−625.44703803	−625.44935917	−625.45255699	−625.45311780
Z	−625.42945147	−625.45755287	−625.46092441	−625.46565929	−625.46650048

Table 4
Dipole moments (μ, in debyes), solvation energies $\Delta E_s = E_{solv} - E_{gas}$, and solvation Gibbs free energies $\Delta G_s = G_{solv} - G_{gas}$ (in kcal/mol) of the DPA forms in the gas phase and solution.

	Gas phase	Chloroform			THF			Methanol			Water		
	μ	ΔE_s	ΔG_s	μ	ΔE_s	ΔG_s	μ	ΔE_s	ΔG_s	μ	ΔE_s	ΔG_s	μ
N	4.03	−7.99	−8.19	4.87	−8.88	−9.11	4.98	−10.12	−10.39	5.13	−10.34	−10.61	5.16
TS	7.83	−13.13	−13.23	8.92	−14.58	−14.70	9.06	−16.59	−16.74	9.24	−16.94	−17.09	9.27
Z	9.37	−17.63	−17.19	11.84	−19.74	−19.28	12.15	−22.71	−22.22	12.58	−23.24	−22.75	12.66

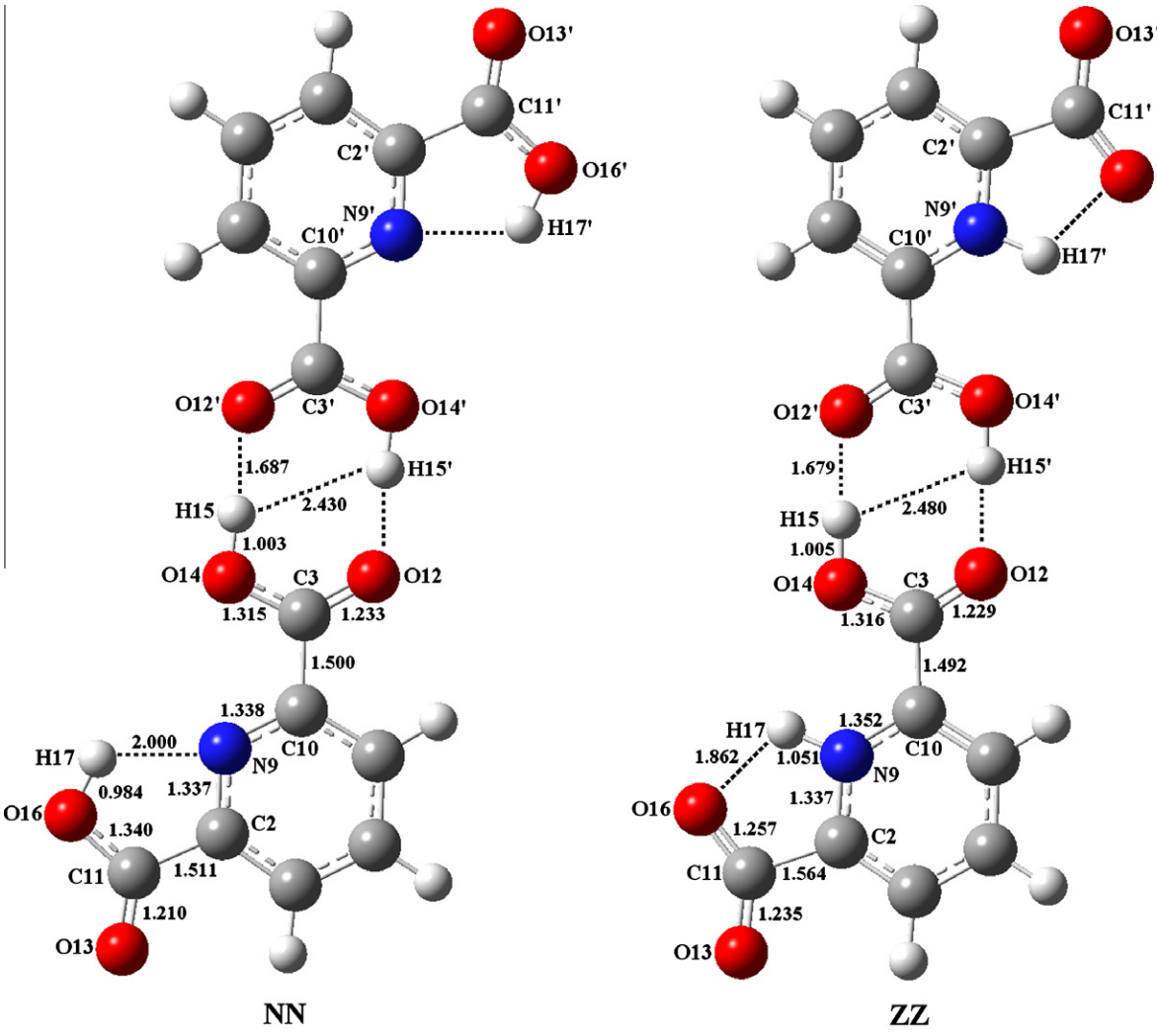

Fig. 3. Optimized structures of the NN and ZZ. Bond lengths are shown in Å and angles in degrees.

0.023 Å (0.019 Å) and 0.019 Å (0.029 Å) longer in NN (ZZ), respectively. The C_3O_{14} and C_3C_{10} bond lengths are 0.026 Å (0.030 Å) and 0.011 Å (0.002 Å) shorter in NN (ZZ), respectively. Additionally, there are changes in the intramolecular hydrogen bonds on going from the monomers to the dimeric structures. The O_{16}—H_{17}···N_9 hydrogen bond length and the O_{16}—H_{17}···N_9 angle are 0.004 Å longer and 0.22° closer in NN. Also, the $C_{11}O_{16}H_{17}$ and $C_2C_{11}O_{16}$ angles are increased by 0.14° and 0.05° in NN, respectively. The N_9—H_{17}···O_{16} hydrogen bond length and the N_9—H_{17}···O_{16} angle are 0.005 Å shorter and 0.07° wider in ZZ, respectively. In addition, the $C_2C_{11}O_{16}$ and C_2N_9 H_{17} angles are decreased by 0.11° and 0.01° in ZZ, respectively.

The values of the calculated uncorrected hydrogen-bonding interaction energies, ΔE, and the corrected interaction energies, ΔE_c, are given in Table 5. The interaction energies are corrected

Table 5
Calculated Gibbs free energies ΔG, interaction energies ΔE, BSSEs, and corrected interaction energies ΔE_c (all in kcal/mol) for the dimerization of the DPA forms, in the gas phase.

Dimer	ΔE	BSSE	ΔE_c	ΔG
NN	−18.86	3.62	−15.24	−6.52
ZZ	−17.83	3.32	−14.51	−5.57

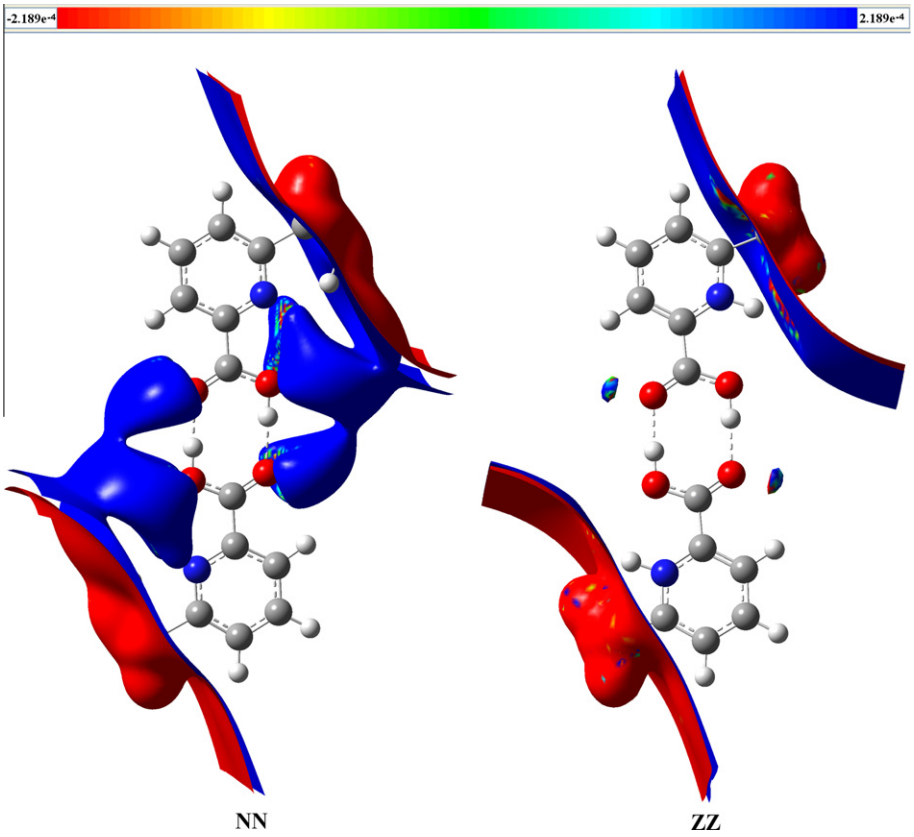

Fig. 4. Electrostatic potential maps for dimers.

for basis set superposition error (BSSE) at the B3LYP level using an approximation to the Boys–Bernardi counterpoise method [66], as described below. The ΔE, of the dimer (for example NN) is defined as

$$\Delta E = E_{N\cdots N} - E_N - E_N$$

where $E_{N\cdots N}$ refers to the total electronic energy of the NN, and E_N is the total electronic energy of N form. When the BSSE is taken into account, the ΔE_c, is then calculated as

$$\Delta E_c = E_{N\cdots N} - E_{E(E\cdots N)}$$

where $E_{N(N\cdots N)}$ is the total electronic energy of monomer N obtained with the extra ghost Gaussian functions placed at the positions of monomer N in the dimer. As seen from these calculated interaction energies, NN and ZZ are stable. The calculated ΔG values in Table 5, show the NN is more stable than ZZ by 0.95 kcal/mol. It is acceptable; however, the intermolecular hydrogen bond lengths in NN are not shorter than those in the ZZ. Therefore, the intermolecular hydrogen bond angels are increased by 1.67° in NN are responsible for this stability. Thus, the stabilities of the dimer structures under investigation can explain importance of the intermolecular hydrogen bonds formed in the dimers.

The molecular electrostatic potential (ESP) is calculated from the charge density (the continuous electron density and the discrete nuclear charge distribution). ESP maps are very useful three dimensional diagrams of molecules. They enable us to visualize the charge distributions and charge related properties of molecules. They also allow us to visualize the size and shape of molecules. There are no grand equations to describe how complex molecules interact with one another, so the best alternative is to use ESP maps. General chemistry focuses very heavily on the charge distributions of molecules. Organic chemistry expands on this molecular property and focuses on reactive sites. Reactive sites are charged regions of a molecule that play a significant role in determining the behavior of other charged molecules in the vicinity. In the majority of the ESP maps, the maximum negative region which is preferred site for electrophilic attack exhibited as red color, while the maximum positive region which is preferred site for nucleophilic attack shown as blue color [68]. In the present study, 3D plots of ESP maps of DPA dimers have been drawn in Fig. 4.

The different values of the electrostatic potential at the surface are represented by different colors. Potential increases in the order red < orange < yellow < green < blue. The color code of these maps is in the range between −0.0002189 a.u. (deepest red) and 0.0002189 a.u. (deepest blue) in compound, where blue shows the relative abundance of electrons and red shows the relative absence of electrons. Comparison of the ESP maps of dimers in the gas phase, indicating intermolecular hydrogen bonds affect the reactive sites. The regions having negative potential are around the terminal COOH groups (NN, ZZ), while the regions having the positive potential are around the central COOH groups and N atoms in the rings (NN). According to the obtained results, it seems intermolecular hydrogen bonds in NN are stronger than those in the ZZ because the higher negative charge density has been used to form them.

4. Conclusions

The major conclusions to be gleaned from this work are as follows:

1. N is more stable than Z in the gas phase and in solution.
2. The barrier height for the proton transfer reaction of DPA decreases upon shifting from the water to the gas phase. As a

result, the intramolecular proton transfer reaction between structures Z and N is thermodynamically and kinetically very easier in the gas phase than in solution.

3. The geometrical parameters of the two monomer molecules in the NN and ZZ structures are nearly the same.
4. Dimerizations of two structures N and Z occur spontaneously, while NN is more favorable than ZZ. That is, the intermolecular hydrogen bonds in the NN structure are stronger than those in the ZZ structure.
5. The results show that the stabilities of the dimer structures are directly affected by the hydrogen bond angels and electrostatic potential value in the dimer structures.
6. There are no published data from computational investigations of the intramolecular proton transfer reactions of DPA and its dimers, so our calculations provide a useful interpretation of data in literature.

Acknowledgment

We are grateful to Ferdowsi University of Mashhad (Iran) for financial support of this work (Grant No. 18071/3-2011/10/04).

References

[1] V.B. Delchev, H. Mikosch, Theoretical study of the intermolecular H-bonding and intermolecular proton transfer between isocytosine tautomeric forms and R, S-lactic acid, J. Mol. Model. 13 (2007) 19–28.
[2] H. Aghabozorg, F. Manteghi, S. Sheshmani, A brief review on structural concepts of novel supramolecular proton transfer compounds and their metal complexes, J. Iran. Chem. Soc. 5 (2008) 184–227.
[3] R.D. Massaro, Y. Dai, E. Blaisten-Barojas, Energetics and vibrational analysis of methyl salicylate isomers, J. Phys. Chem. A 113 (2009) 10385–10390.
[4] N. Tezer, N. Karakus, Theoretical study on the ground state intramolecular proton transfer (IPT) and solvation effect in two Schiff bases formed by 2-aminopyridine with 2-hydroxy-1-naphthaldehyde and 2-hydroxy salicylaldehyde, J. Mol. Model. 15 (2009) 223–232.
[5] S. Ash, S.P. De, S. Pyne, A. Misra, Excited state intramolecular proton transfer in 3-hydroxy flavone and 5-hydroxy flavone: a DFT based comparative study, J. Mol. Model. 16 (2010) 831–839.
[6] D.Ö. Isin, N. Karakus, Computational study of the intramolecular proton transfer reactions of 3-hydroxytropolone (2,7-dihydroxycyclohepta-2,4,6-trien-1-one) and its dimers, J. Mol. Model. 16 (2010) 1877–1882.
[7] B.D. Vassil, Computational (DFT and TD DFT) study of the electron structure of the tautomers/conformers of uridine and deoxyuridine and the processes of intramolecular proton transfers, J. Mol. Model. 16 (2010) 749–757.
[8] M.J. Tenorio, M.C. Puerta, P. Valerga, S. Moncho, G. Ujaque, A. Lledós, Proton-transfer reactions to half-sandwich ruthenium trihydride complexes bearing hemilabile P, N ligands: experimental and density functional theory studies, Inorg. Chem. 49 (2010) 6035–6057.
[9] R.D. Massaro, Y. Dai, E. Blaisten-Barojas, Theoretical investigation of the photophysics of methyl salicylate isomers, J. Chem. Phys. 135 (2011) 164306.
[10] P. Borowski, R. Gawinecki, A. Miłaczewska, A. Skotnicka, K. Woliński, A. Brzyska, Instability of 2,2-di(pyridin-2-yl)acetic acid. Tautomerization versus decarboxylation, J. Mol. Model. 17 (2011) 857–868.
[11] M. Mirzaei, H. Aghabozorg, H. Eshtiagh-Hosseini, A brief review of structural concepts of novel supramolecular proton transfer compounds and their metal complexes (part II), J. Iran. Chem. Soc. 8 (2011) 580–607.
[12] I. Majerz, M.J. Gutmann, Mechanism of proton transfer in the strong OHN intermolecular hydrogen bond, RSC Adv. 1 (2011) 219–228.
[13] V. Enchev, S. Angelova, M. Rogojerov, V. Monev, I. Wawer, M. Tkaczyk, K. Kostova, Solid-state tautomerism in 2-carboxyindan-1,3-dione, J. Phys. Chem. A 115 (2011) 2026–2034.
[14] B.J. Ośmiałowski, Proton transfer reaction and intermolecular interactions in associates of 2,5-dihydroxy-1,8-naphthyridine, J. Mol. Model. 18 (2012) 1633–1644.
[15] S. Udo, Studies on the constituents of natto the fermented soybeans part I, J. Agric. Chem. Soc. Jpn. 12 (1936) 386–394.
[16] J. Powell, R. Strange, Biochemical changes occurring during the germination of bacterial spores, Biochem. J. 54 (1953) 205–209.
[17] J. Powell, Isolation of dipicolinic acid (pyridine-2:6-dicarboxylic acid) from spores of bacillus megatherium, Biochem. J. 54 (1953) 210–211.
[18] D. Rosen, C. Sharpless, L. McGown, Bacterial spore detection and determination by use of terbium dipicolinate photoluminescence, Anal. Chem. 69 (1997) 1082–1085.
[19] A.A. Hindle, E.A.H. Hall, Dipicolinic acid (DPA) assay revisited and appraised for spore detection, Analyst 124 (1999) 1599–1604.
[20] J. Anderson, J. Nelson, C. Reynolds, D. Ringelberg, G. Tepper, D. Pestov, Steady-state and frequency-domain lifetime measurements of an activated molecular imprinted polymer imprinted to dipicolinic acid, J. Fluorine 14 (2004) 269–274.
[21] S. Sarasanandarajah, J. Kunnil, B. Bronk, L. Reinisch, Two-dimensional multiwavelength fluorescence spectra of dipicolinic acid and calcium dipicolinate, Appl. Opt. 44 (2005) 1182–1187.
[22] V.H. Holsinger, L.C. Blankenship, M.J. Pallansch, Ultraviolet absorption by dipicolinic acid in model systems and bacterial spores, Arch. Biochem. Biophys. 119 (1967) 282–287.
[23] P. Carmona, Vibrational spectra and structure of crystalline dipicolinic acid and calcium dipicolinate trihydrate, Spectrochim. Acta. A 36 (1980) 705–712.
[24] E. Ghiamati, R. Mancharan, W.H. Nelson, J.F. Sperry, UV resonance Raman spectra of bacillus spores, Appl. Spectrosc. 46 (1992) 357–364.
[25] H.F. Hameka, J.O. Jensen, J.L. Jensen, C.N. Merrow, C.P. Vlahacos, Theoretical studies of the fluorescence of dipicolinic acid and its anion, J. Mol. Struct. (THEOCHEM) 365 (1996) 131–141.
[26] R. Nudelman, B. Bronk, S. Efrima, Fluorescence emission derived from dipicolinic acid, its sodium and its calcium salts, Appl. Spectrosc. 54 (2000) 445–449.
[27] A.A. Kolomenskii, S.N. Jerebtsov, T. Opatrny, H.A. Schuessler, M.O. Scully, Spontaneous Raman spectra of dipicolinic acid in microcrystalline form, J. Mod. Opt. 50 (2003) 2369–2374.
[28] A.A. Kolomenskii, H.A. Schuessler, Raman spectra of dipicolinic acid in crystalline and liquid environments, Spectrochim. Acta. A 61 (2005) 647–651.
[29] J.R. Xie, V.H. Smith Jr., R.E. Allen, Spectroscopic properties of dipicolinic acid and its dianion, Chem. Phys. 322 (2006) 254–268.
[30] K. McCann, J. Laane, Raman and infrared spectra and theoretical calculations of dipicolinic acid, dinicotinic acid and their dianions, J. Mol. Struct. 890 (2008) 346–358.
[31] G. Strahs, R.E. Dickerson, The crystal structure of calcium dipicolinate trihydrate (a bacterial spore metabolite), Acta Cryst. B 24 (1968) 571–578.
[32] F. Takusagawa, K. Hirotsu, A. Shimada, The crystal structure of dipicolinic acid monohydrate, Bull. Chem. Soc. Jpn. 46 (1973) 2020–2027.
[33] V.C. Tellez, B.S. Gaytan, S. Bernes, E.G. Vergara, The supramolecular structure of pyridine-2,6-dicarboxylic acid, Acta Cryst. C 58 (2002) 228–230.
[34] R.D. Massaro, E. Blaisten-Barojas, Density functional theory study of dipicolinic acid isomers and crystalline polytypes, Comput. Theor. Chem. 977 (2011) 148–156.
[35] S.V. Konovalikhin, P.Ya. Boikov, E.B. Burlakova, The bimodal physiological effect of certain picolinic acid derivatives is due to the specific structure of zwitterions, Biol. Bull. 28 (2001) 191–195.
[36] F. Peral, E. Gallego, Self-association of pyridine-2,6-dicarboxylic acid in aqueous solution as determined from ultraviolet hypochromic and hyperchromic effects, Spectrochim. Acta. A 56 (2000) 2149–2155.
[37] A. Moghimi, M.A. Sharif, H. Aghabozorg, Creatininium dipicolinate monohydrate, Acta Cryst. E 60 (2004) o1790–o1792.
[38] H. Aghabozorg, A. Akbari Saei, F. Ramezanipour, 2,6-Diaminopyridinium pyridinium-2,6-dicarboxylate: a redetermination, Acta Cryst. E 61 (2005) o3242–o3244.
[39] S. Sheshmani, M. Ghadermazi, H. Aghabozorg, Piperazinium bis(6-carboxypyridine-2-carboxylate) trihydrate, Acta Cryst. E 62 (2006) o3620–o3622.
[40] H. Aghabozorg, M. Ghadermazi, S. Sheshmani, Crystal structure of a proton-transfer self-associated compound: benzene-1,3-diaminium bis(hydrogen pyridine-2,6-carboxylate) dihydrate, Anal. Sci. 22 (2006) x231–x232.
[41] H. Aghabozorg, M. Ghadermazi, E. Sadr-khanlou, Crystal structure of piperazine and pyridine-2,6-dicarboxylic acid complex, Anal. Sci. 22 (2006) x253–x254.
[42] A. Moghimi, V. Lippolis, H. Aghabozorg, A. Shokrollahi, M. Shamsipur, S. Sheshmani, A.J. Blake, Characterization, crystal structure, and solution studies of a proton transfer compound obtained from 2,6-pyridinedicarboxylic acid and 1,4,10,13-tetraoxa-7,16-diazacyclooctadecane, Pol. J. Chem. 80 (2006) 1385–1396.
[43] H. Aghabozorg, F. Manteghi, M. Ghadermazi, Ammonium 6-carboxypyridine-2-carboxylate, Acta Cryst. E 63 (2007) o4454.
[44] J. Soleimannejad, H. Aghabozorg, E. Motieiyan, M. Ghadermazi, J. Attar Gharamaleki, H. Adams, Propane-1,3-diaminium–2-carboxypyridine–6-carboxylate-pyridine–2,6-dicarboxylic acid-water (1/2/2/8), Acta Cryst. E 64 (2008) o231–o232.
[45] H. Aghabozorg, M. Heidari, M. Ghadermazi, J. Attar Gharamaleki, Propane-1,2-diammonium bis-(6-carboxy-pyridine-2-carboxyl-ate) dehydrate, Acta Cryst. E 64 (2008) o1045–o1046.
[46] A. Delori, V.R. Pedireddi, PKa directed host-guest assemblies of 2,4-diamino-6-methyl-triazine with various dicarboxylic acids, Acta Cryst. A 64 (2008) C480.
[47] H. Aghabozorg, E. Motieiyan, A.R. Salimi, M. Mirzaei, F. Manteghi, A. Shokrollahi, S. Derki, M. Ghadermazi, S. Sheshmani, H. Eshtiagh-Hosseini, Piperazinediium, Zr(IV) and Ce(IV) pyridine-2,6-dicarboxylates: syntheses, characterizations, crystal structures, ab initio HF, DFT calculations and solution studies, Polyhedron 29 (2010) 1453–1464.
[48] M.A. Sharif, M. Tabatabaee, M. Adinehloo, H. Aghabozorg, 2-Amino-4-methyl-pyridinium 6-carb-oxy-pyridine-2-carboxyl-ate sesquihydrate, Acta Cryst. E 66 (2010) o3232.
[49] A. Moghimi, M. Ranjbar, H. Aghabozorg, F. Jalali, M. Shamsipur, R.K. Chadha, NMR characterization, X-Ray crystal structure and solution studies of Ni(II)

complexes of a pyridine containing self-assembling system, J. Chem. Res. (2002) 1047–1065.
[50] M. Ranjbar, A. Moghimi, H. Aghabozorg, G.P.A. Yap, Crystal structure of zinc(II) complex of a pyridine containing self-assembling system, Anal. Sci. 18 (2002) 219–220.
[51] A. Moghimi, S. Sheshmani, A. Shokrollahi, M. Shamsipur, G. Kickelbick, H. Aghabozorg, Crystal structures and solution studies of two novel zinc(II) complexes of a proton transfer compound obtained from 2,6-pyridinedicarboxylic acid and 1,10-phenanthroline: observation of strong intermolecular hydrogen bonds, Z. Anorg. Allg. Chem. 631 (2005) 160–169.
[52] F. Ramezanipour, H. Aghabozorg, A. Shokrollahi, M. Shamsipur, H. Stoeckli-Evans, J. Soleimannejad, S. Sheshmani, Different complexation behavior of a proton transfer compound obtained from 1,10-phenanthroline and pyridine-2,6-dicarboxylic acid with InIII and CeIII: synthesis, crystal structures and solution studies, J. Mol. Struct. 779 (2005) 77–86.
[53] H. Aghabozorg, F. Ramezanipour, P.D. Kheirollahi, A.A. Saei, A. Shokrollahi, M. Shamsipur, F. Manteghi, J. Soleimannejad, M.A. Sharif, Novel complexes of gallium(III), indium(III), and thallium(III) with pyridine-containing proton transfer ion pairs obtained from dipicolinic acid-synthesis, characterization and X-ray crystal structure, Z. Anorg. Allg. Chem. 632 (2006) 147–154.
[54] H. Aghabozorg, F. Ramezanipour, B. Nakhjavan, J. Soleimannejad, J. Attar Gharamaleki, M.A. Sharif, Different complexation behavior of a proton transfer compound obtained from 1,10-phenanthroline and pyridine-2, 6-dicarboxylic acid with Sn(IV), Sb(III) and Tl(I), J. Cryst. Res. Technol. 42 (2007)
1137–1144.
[55] H. Aghabozorg, E. Sadr-khanlou, Synthesis, characterization and X-ray crystal structure of guanidinuim (pyridine-2,6-dicarboxylato)(pyridine-2, 6-monocarboxylato) zincate(II) mono pyridine-2,6-dicarboxylic acid tetrahydrate, Cryst. Res. Technol. 43 (2008) 327–332.
[56] H. Aghabozorg, F. Ramezanipour, J. Soleimannejad, M.A. Sharif, A. Shokrollahi, M. Shamsipur, A. Moghimi, J. Attar Gharamaleki, V. Lippolis, A.J. Blake, Different complexation behavior of a proton transfer compound obtained from pyridine-2,6-dicarboxylic acid and creatinine with Tl(I), Cu(II), Fe(III) and Bi(III): synthesis, characterization, crystal structures and solution studies, Pol. J. Chem. 82 (2008) 487–507.
[57] M. Tabatabaee, H. Aghabozorg, J. Attar Gharamaleki, M.A. Sharif, Acridinium (6-carboxy-pyridine-2-carboxyl-ato)(pyridine-2,6-dicarboxyl-ato)zincate(II) penta-hydrate, Acta Cryst. E 65 (2009) m473–m474.
[58] J. Soleimannejad, H. Aghabozorg, S. Hooshmand, M. Ghanbari, F. Manteghi, M. Shamsipur, Two novel metal organic frameworks of Sn(II) and Pb(II) with pyridine-2,6-dicarboxylic acid and 4,4′-bipyridine: syntheses, crystal structures and solution studies, J. Iran. Chem. Soc. 7 (2010) 405–418.
[59] H. Pasdar, S. Heidari, H. Aghabozorg, B. Notash, Hexaaquamagnesium(II) bis(pyridinium-2,6-dicarboxylate), Acta Cryst. E 66 (2010) m1581.
[60] H. Aghabozorg, S. Omidvar, M. Mirzaei, B. Notash, Crystal structure of 4,4′-bipyridinium bis(pyridine-2,6-dicarboxylato) mercurate(II)–diaquabis(6-carboxypyridine-2-carboxylato) mercury(II)–water (2:1:12), $[C_{10}H_{10}N_2]_2[Hg(C_7H_3NO_4)_2]_2$ $Hg(H_2O)_2(C_7H_4NO_4)_2$ $12H_2O$, Z. Kristallogr. NCS 226 (2011) 123–125.
[61] M.C. Grossel, A.N. Dwyer, M.B. Hursthouse, J.B. Orton, Polymorphism in pyridine-2,6-dicarboxylic acid: competition between robust synthons, Cryst. Eng. Commun. 8 (2006) 123–128.
[62] C. Lee, W. Yang, P.G. Parr, Development of the colle-salvetti correlation-energy formula into a functional of the electron density, Phys. Rev. B 37 (1988) 785–789.
[63] A.D. Becke, Density functional thermochemistry.III. The role of exact exchange, J. Chem. Phys. 98 (1993) 5648.
[64] A.D. Becke, Density functional exchange-energy approximation with correct asymptotic behavior, Phys. Rev. A 38 (1988) 3098–3100.
[65] V. Barone, M. Cossi, Quantum calculation of molecular energies and energy gradients in solution by a conductor solvent model, J. Phys. Chem. A 102 (1998) 1995–2001.
[66] S.F. Boys, F. Bernardi, The calculation of small molecular interactions by the differences of separate total energies. some procedures with reduced errors, Mol. Phys. 19 (1970) 553–566.
[67] M.J. Frisch, G.W. Trucks, H.B. Schlegel, et al., GAUSSIAN 09, Gaussian, Inc., Wallingford, CT, 2009.
[68] M. Karabacak, E. Kose, A. Atac, Molecular structure (monomeric and dimeric structure) and HOMO–LUMO analysis of 2-aminonicotinic acid: a comparison of calculated spectroscopic properties with FT-IR and UV–vis, Spectrochim. Acta. A 91 (2012) 83–96.